

## Phase Diagram of Liquid $^3\text{He}$ between 0.7 and 2.5 mK

A. I. Ahonen, M. T. Haikala, M. Krusius, and O. V. Lounasmaa

*Low Temperature Laboratory, Helsinki University of Technology, SF-02150 Otaniemi, Finland*

(Received 8 July 1974)

We describe a nuclear demagnetization cryostat in which liquid  $^3\text{He}$  has been cooled to below 0.7 mK. Data on the boundaries between the normal Fermi-liquid and the superfluid phases of  $^3\text{He}$ , as determined from NMR measurements, are presented between 0.7 and 2.5 mK and from 0 to 27 bar. The " $\lambda$  point" of  $^3\text{He}$  was found at 0.93 mK.

Wheatley and co-workers<sup>1</sup> have previously determined the phase diagram of liquid  $^3\text{He}$  above 1.9 mK and 10 bar pressure. By employing nuclear refrigeration techniques we have extended this work to lower temperatures and pressures, including the saturated vapor pressure. In connection with these experiments liquid  $^3\text{He}$  was cooled to 0.7 mK, lower than ever before. A considerable effort was made to measure the temperature of  $^3\text{He}$  directly.

Adiabatic demagnetization of the nuclear spins of a suitable metal<sup>2,3</sup> is a method whereby liquid  $^3\text{He}$  can, in principle, be cooled well into the microkelvin region. A drawback of this method is that the cryostat is necessarily quite complicated because a low starting temperature, below 20 mK, and a high initial magnetic field, over 5 T, are required for successful nuclear demagnetization.

Furthermore, it was thought that the high Kapitza thermal boundary resistance, assumed proportional to  $1/T^3$ , between liquid helium and a metal would prevent the use of nuclear refrigeration for cooling  $^3\text{He}$  below 2 mK. Subsequently it was observed,<sup>4</sup> however, that the heat resistance is smaller than expected, exhibiting a relatively weak  $1/T$  temperature dependence below 10 mK. The low thermal boundary resistance is presumably due to a magnetic interaction between the nuclear spins of  $^3\text{He}$  and the electronic impurity moments of the metal. This additional thermal coupling is of paramount importance for nuclear refrigeration of liquid  $^3\text{He}$ .

Our cryostat is illustrated in Fig. 1. The nuclear stage is made of a bundle of 0.1-mm-diam copper wires containing a total of 22 moles of copper; the bundle was made stiff by epoxy. Highest purity wire, having a resistance ratio  $R(300\text{ K})/R(4\text{ K})=150$ , was used. The wires were welded at their top end to a copper piece which, in turn, was welded to the  $^3\text{He}$  cell.

In order to achieve good thermal contact between liquid  $^3\text{He}$  and the nuclear refrigerant, the

cell was sintered full of copper powder<sup>5</sup> with a 40% packing factor, except for a cylindrical space occupied by the NMR coils. The main magnetic impurities of the powder are 200 ppm of iron and 4.4 ppm of manganese; it is believed that manganese is the more important element in reducing the thermal boundary resistance to  $^3\text{He}$ . With 28 g of sinter in the cell the total surface area for heat exchange is  $30\text{ m}^2$ ; the space available for liquid  $^3\text{He}$  is  $6\text{ cm}^3$ . Because the bulk thermal conductivity of the sinter is relatively poor the  $^3\text{He}$  chamber was equipped with sixteen copper rods of 2 mm diameter, welded to the bottom of the cell. Highest-purity copper was employed for constructing the  $^3\text{He}$  cell and other

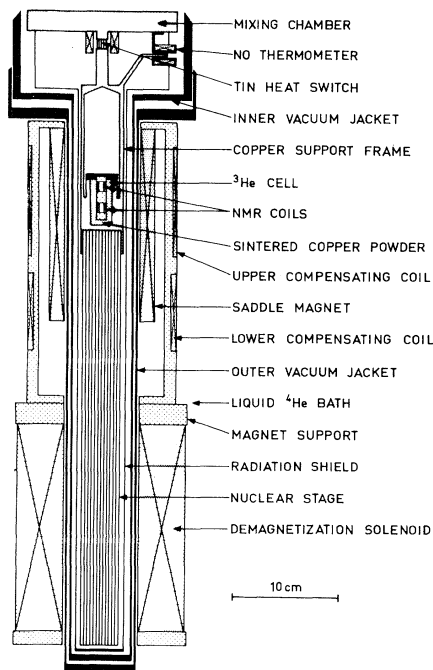


FIG. 1. Schematic illustration of the lower part of the cryostat showing the mixing chamber of the pre-cooling dilution refrigerator, the  $^3\text{He}$  cell, and the nuclear stage.

parts through which heat must flow.

A 7.5-T superconducting solenoid is used for nuclear demagnetization; it incorporates two compensating coils which cancel, over the region of the  $^3\text{He}$  cell, the field produced by the main solenoid. The smaller coils as well as the relatively large distance between the demagnetization solenoid and the cell ensure that the field applied to liquid  $^3\text{He}$  can be varied independently.

Two 7-mm-long NMR coils, each wound on an epoxy former 14 mm long and with a 4.5 mm i.d., are located on the center axis of the  $^3\text{He}$  cell. The upper one is filled to 35% by volume with platinum powder of 8  $\mu\text{m}$  average diameter; it is used for thermometry by observing the NMR signal of platinum, and also for measurements on  $^3\text{He}$ . The lower resonance coil contains only  $^3\text{He}$ .

The static magnetic field for NMR measurements is generated by means of a saddle magnet made of two coils which produce a field transverse to the vertical axis of the NMR coils. The overall field homogeneity  $\Delta B/B$  is  $6 \times 10^{-4}$  as determined from the linewidth of the  $^3\text{He}$  resonance signal. NMR measurements on liquid  $^3\text{He}$  were made by sweeping the static field and by frequency modulating the rf excitation; low-frequency phase-sensitive detection techniques could thus be employed.

Our pulsed NMR thermometer<sup>6</sup> was self-calibrated via an automated measurement of the nuclear spin-lattice relaxation time  $\tau_1$  of  $^{195}\text{Pt}$  and by the use of Korringa's relation,  $\tau_1 T_e = 29.8$  msec K;  $T_e$  is the lattice and conduction-electron temperature of platinum. The measuring procedure was to find the calibration constant  $A$  in Curie's relation  $\chi_n = A/T_n$  from relaxation-time measurements between 2 and 4 mK; here  $\chi_n$  is the dynamic nuclear susceptibility and  $T_n$  the nuclear spin temperature of platinum. Above 5 mK the platinum thermometer could also be checked against a nuclear orientation thermometer, based on the anisotropy of  $\gamma$  rays emitted by oriented  $^{54}\text{Mn}$  nuclei in nickel. It should be noted that a pulsed NMR thermometer measures the temperature just before the pulse; the readings are thus equilibrium temperatures and unaffected by transients. We also want to emphasize that the platinum powder is in thermal contact with liquid  $^3\text{He}$  only; our thermometer thus measures the  $^3\text{He}$  temperature directly. This is an important improvement over some of the earlier nuclear refrigeration experiments.<sup>2</sup>

A dilution refrigerator cools the nuclear stage

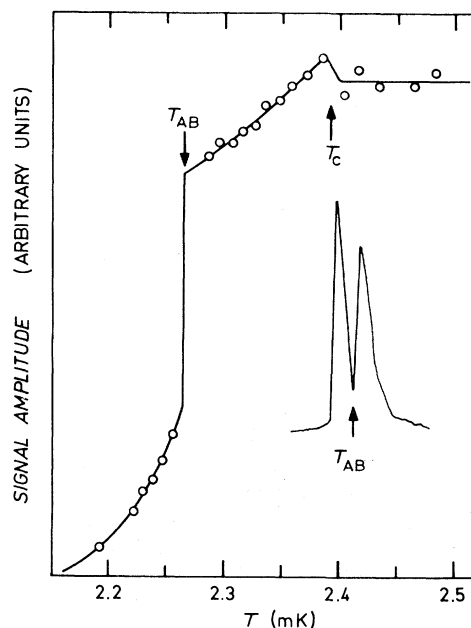


FIG. 2. The maximum resonance amplitude as a function of temperature near  $T_c$  and  $T_{AB}$  for  $P = 22.4$  bar. Between 2.4 and 2.2 mK the amplitude decreases by 40%. The inset shows the NMR signal at  $T_{AB}$ ; the transition from the A to the B phase happens to occur in the middle of a resonance peak.

to 17 mK. Demagnetization from 7.5 T to a final field between 0.05 and 0.1 T is then performed in 3.5 h, and liquid  $^3\text{He}$  reaches its lowest temperature, presently slightly below 0.7 mK, in 4 h; the subsequent warm-up time to 1.0 mK, caused by an external heat leak of 0.2 nW per mole of copper, is 20 h.

Our transverse NMR measurements were performed in a static field of 32 mT. The signal was recorded both upon cooling and during subsequent warming through the phase transitions which were identified by changes in the signal amplitude. Above 20 bar, the A phase could also be recognized from a shift of the resonant frequency.<sup>7</sup>

Figure 2 illustrates a typical behavior of the NMR signal. Upon crossing the second-order phase boundary from the normal Fermi liquid into the A phase at  $T_c$ , the amplitude first increased a few per cent and then slowly started to decrease. These variations in the maximum absorption are caused by changes in the line shape; the total area under the resonance curve appears to be roughly constant within our resolution. At the first-order transition between the A and B phases the amplitude changed discontinu-

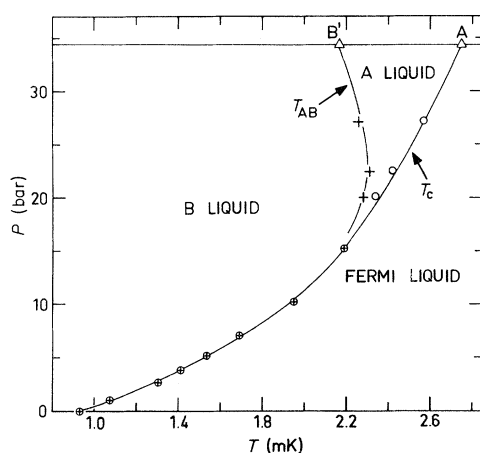


FIG. 3. The phase diagram of liquid  ${}^3\text{He}$ . Our data at 32 mT: open circles,  $T_c$ ; crosses,  $T_{AB}$ ; crosses in circles, "average" of  $T_c$  and  $T_{AB}$ . Triangles, melting-curve data from Ref. 8.

ously and then decreased rapidly in the  $B$  phase. The transition temperature  $T_{AB}$  could be determined, above 20 bar, only upon warming because substantial supercooling always occurred; superheating was never observed in the lower coil containing bulk liquid. In order to avoid thermal inhomogeneities, the temperature was varied slowly,  $50 \mu\text{K}/\text{h}$ , through the transition region. In most cases  $T_{AB}$  and  $T_c$  could be determined with a precision of  $30 \mu\text{K}$ .

By tracing the NMR signals as a function of temperature at different pressures we have determined the phase diagram of liquid  ${}^3\text{He}$ ; the results are shown in Fig. 3. Below 15 bar the  $A$  phase becomes so narrow that the resolution of our NMR measurements is not sufficient for distinguishing between  $T_c$  and  $T_{AB}$ . At these pressures the measured transition temperature thus corresponds to an "average" of  $T_c$  and  $T_{AB}$ ; the transition was identified by a discontinuity in the temperature derivative of the resonance amplitude.

We observe that the boundary between the normal Fermi-liquid region and the superfluid phases is smooth all the way to the saturated vapor pressure, which probably means that the main features of the phase diagram have by now been observed. The " $\lambda$  point" of  ${}^3\text{He}$ , i.e.,  $T_c$  at zero pressure, is at  $0.93 \text{ mK}$ . The precision of our transition temperatures on the platinum NMR scale is about  $0.02 \text{ mK}$ . We have also plotted in Fig. 3 the transition points on the melting curve

as determined recently by Halperin *et al.*<sup>8</sup> from thermodynamic measurements.

The phase diagram of liquid  ${}^3\text{He}$  has previously been investigated above  $1.9 \text{ mK}$  by Wheatley and co-workers<sup>1</sup>; discontinuities in the temperature derivatives of heat flow and static magnetic susceptibility were employed for identifying the phase boundaries. For the sake of clarity these results have not been included in Fig. 3 but the agreement with our data, especially below 20 bar, is surprisingly good. The same transition temperatures for the second-order phase change at  $T_c$  were also obtained from resonance data on liquid  ${}^3\text{He}$  intermixed with  $8\text{-}\mu\text{m}$  platinum powder.<sup>3</sup> There are indications that in the  $A$  phase  $T_c$  is pushed towards lower temperatures for some of the liquid within the powder. This interpretation of the data is based on the fact that both an unshifted and a shifted resonance line are simultaneously observed in the  $A$ -phase region; the intensity of the former signal decreases rapidly towards lower temperatures.

It appears from our data that the thermal relaxation time between liquid  ${}^3\text{He}$  and the nuclear stage is not increasing significantly upon cooling. This gives us hope that even lower temperatures can be achieved by nuclear refrigeration of liquid  ${}^3\text{He}$ . It also seems that the temperature of liquid  ${}^3\text{He}$  below  $1 \text{ mK}$  can be measured reliably by the platinum-powder NMR thermometer, although further investigations are required.

Finally, it should be pointed out that nuclear refrigeration now has made possible experiments involving the free surface of superfluid  ${}^3\text{He}$ .

We wish to thank T. A. Alvesalo, D. S. Fisher, M. S. Grönstrand, U. A. Lähteenmäki, and E. Turtiainen for help with the experiments and in analyzing the data.

<sup>1</sup>T. J. Greytak, R. T. Johnson, D. N. Paulson, and J. C. Wheatley, *Phys. Rev. Lett.*, **31**, 452 (1973); D. N. Paulson, R. T. Johnson, and J. C. Wheatley, *Phys. Rev. Lett.*, **31**, 746 (1973); D. N. Paulson, H. Kojima, and J. C. Wheatley, *Phys. Rev. Lett.*, **32**, 1098 (1974).

<sup>2</sup>J. M. Dundon, D. L. Stofa, and J. M. Goodkind, *Phys. Rev. Lett.*, **30**, 843 (1973).

<sup>3</sup>A. I. Ahonen, M. T. Haikala, and M. Krusius, *Phys. Lett.*, **47A**, 215 (1974).

<sup>4</sup>O. Avenel, M. P. Berglund, R. G. Gylling, N. E. Phillips, A. Vetleseter, and M. Vuorio, *Phys. Rev. Lett.*, **31**, 76 (1973).

<sup>5</sup>The copper powder was purchased from Wolstenholme Bronze Powders Ltd., Bolton, Lancashire,

England. It is in the form of flakes which are  $2\ \mu\text{m}$  thick and 20 to  $50\ \mu\text{m}$  in diameter.

<sup>6</sup>M. I. Aalto, H. K. Collan, R. G. Gylling, and K. O. Nores, *Rev. Sci. Instrum.* **44**, 1075 (1973).

<sup>7</sup>D. D. Osheroff, W. J. Gully, R. C. Richardson, and

D. M. Lee, *Phys. Rev. Lett.* **29**, 920 (1972).

<sup>8</sup>W. P. Halperin, C. N. Archie, F. B. Rasmussen, and R. C. Richardson, to be published; W. P. Halperin, R. A. Buhrman, D. M. Lee, and R. C. Richardson, *Phys. Lett.* **45A**, 233 (1973).

## Superfluid Mass of Liquid Helium Three\*

A. W. Yanof and J. D. Reppy

*Laboratory of Atomic and Solid State Physics and The Materials Science Center,  
Cornell University, Ithaca, New York 14850*

(Received 8 July 1974)

Fourth sound has been generated and detected in the superfluid phases of liquid  $^3\text{He}$  by means of a new technique.

The discovery of transitions to new phases of liquid  $^3\text{He}$  in the millikelvin temperature range by Osheroff *et al.*<sup>1</sup> revitalized old speculations about the possible superfluidity of liquid  $^3\text{He}$ . A convincing demonstration of superfluidity has been provided by measurements of fourth-sound modes in liquid  $^3\text{He}$  by Kojima, Paulson, and Wheatley,<sup>2</sup> and more recently by our group.<sup>3</sup>

Kojima, Paulson, and Wheatley<sup>2</sup> have employed the technique developed by Shapiro and Rudnick<sup>4</sup> to obtain the fourth-sound velocity. The porous medium used is a compressed powder of cerium magnesium nitrate (CMN) which also serves as a refrigerant and thermometer. Drawing a reasonable analogy to fourth sound in  $^4\text{He}$ , Kojima, Paulson, and Wheatley<sup>2</sup> interpret their results in terms of simple two-fluid hydrodynamics and obtain the superfluid fraction  $\rho_s/\rho$  from the expression<sup>4</sup>

$$\rho_s/\rho = n^2(c_4/c_1)^2, \quad (1)$$

where  $c_4$  is the measured velocity of fourth sound and  $c_1$  is the velocity of ordinary sound in bulk liquid. The factor  $n^2$  is a correction term which arises from the complex geometry of the porous medium through which the fourth sound must propagate.

In the work reported here, we employ the method developed by Hall, Kiewiet, and Reppy.<sup>5</sup> Fourth sound is generated by oscillating the entire sample chamber. The liquid properties are then deduced from the response of the sample chamber to a known applied force, and the inertial mass of the oscillating superfluid is obtained directly. This independent measurement can be compared to the value of superfluid density obtained from Eq. (1), thus giving a partial test of

the validity of the simple two-fluid model for  $^3\text{He}$ .

The apparatus is shown in Fig. 1. A cylindrical sample chamber, packed with CMN powder, is suspended elastically by an epoxy rod inside a massive epoxy incasement. An electrode mounted in the incasement drives the cell electrostatically along the cylinder axis. The resulting cell displacement  $X$  is sensed electrostatically and monitored by two lock-in amplifiers in quadrature.

Figure 2(a) shows the frequency response with the cell filled with liquid  $^4\text{He}$  at a temperature of 0.5 K. At 0.7 kHz a suspension resonance is seen. Here the cell oscillates along its axis at

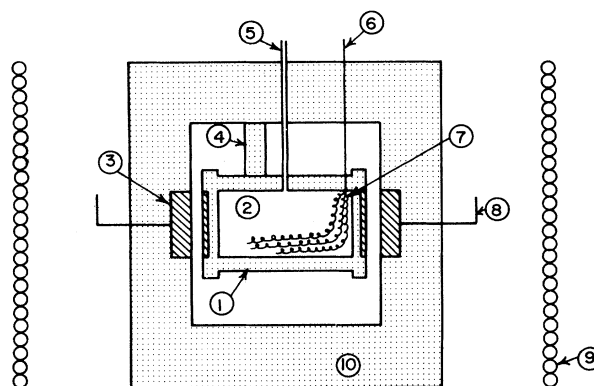


FIG. 1. Schematic diagram of fourth-sound apparatus. 1, Epoxy sample chamber; 2, packed powder (see Ref. 4); 3, metal electrode for driving cavity electrostatically; 4, epoxy suspension rod; 5, fill capillary; 6, high-purity copper wire to heat switch and mixing chamber; 7, wire brush ( $40\ \text{cm}^2$  surface area); 8, electrode for detecting cavity motion; 9, susceptibility coils and solenoid for magnetic cooling; 10, massive epoxy incasement.